Soft Matter

PAPER

View Article Online
View Journal | View Issue

Cite this: *Soft Matter*, 2024, **20**, 2464

Stability of the chiral crystal phase and breakdown of the cholesteric phase in mixtures of active–passive chiral rods†

Jayeeta Chattopadhyay, ‡§ Jaydeep Mandal‡ and Prabal K. Maiti *

Received 18th November 2023,
Accepted 7th February 2024

DOI: 10.1039/d3sm01567j

rsc.li/soft-matter-journal

In this study, we aim to explore the effect of chirality on the phase behavior of active helical particles driven by two-temperature scalar activity. We first calculate the equation of state of soft helical particles of various intrinsic chiralities using molecular dynamics (MD) simulation. In equilibrium, the emergence of various liquid crystal (LC) phases such as nematic (*N*), cholesteric (N_c^*), smectic (Sm) and crystal (*K*) crucially depends on the presence of walls that induce planar alignment. Next, we introduce activity through the two-temperature model: keep increasing the temperature of half of the helical particles (labeled as 'hot' particles) while maintaining the temperature of the other half at a lower value (labeled as 'cold' particles). Starting from a homogeneous isotropic (*I*) phase, we find the emergence of 2-TIPS: two temperature-induced phase separations between the hot and cold particles. We also observe that the cold particles undergo an ordering transition to various LC phases even in the absence of a wall. This observation reveals that the hot–cold interface in the active system plays the role of a wall in the equilibrium system by inducing an alignment direction for the cold particles. However, in the case of a cholesteric phase, we observe that activity destabilizes the N_c^* phase by inducing smectic ordering in the cold zone while an isotropic structure in the hot zone. The smectic ordering in the cold zone eventually transforms to a chiral crystal phase with high enough activity.

1 Introduction

Understanding how chirality spreads from the molecular scale to the macroscopic scale is important due to its immense contribution to basic science and industrial applications. Chiral particles that only interact sterically are one particularly intriguing example. Helix is one of the most basic models in this class that gives rise to the cholesteric phase (or chiral nematic),[1–3] in which particles undergo rotation around a specific helical axis. The wavelength associated with this rotation is called the pitch of the macroscopic cholesteric phase P_{chol}. This wavelength can have values that are many orders of magnitude larger than the molecular size. Cholesteric phases can be observed in different systems like DNA,[4–6] fd viruses,[7] amyloid fibrils[8] and others.[9–11] They have applications in wide areas of optoelectronic technology.[12] Another important aspect of the cholesteric phases is the sense of rotation or handedness. It is important to study the relationship between the intrinsic helicity of the molecules and the macroscopic chiral phase. Right-handed DNA forms a left-handed chiral macrophase.[13] Left-handed filamentous viruses are observed to form right-handed cholesteric phases.[11] Liquid crystal ordering can be seen in ultrashort double-stranded DNA[14] and RNA,[15] which are right-handed helices.

Different theoretical and computational models have been proposed to understand the link between molecular and macroscopic chirality. Theoretical studies have been used to predict the pitch of the cholesteric phase.[16] Odijk[17] has studied the pitch of the cholesteric phase using particle models where rod-like particles are enveloped by thin chiral threads. Using the corkscrew model, Pelcovits[18] showed that the pitch of the cholesteric phase is independent of the flexibility of the molecules, but depends on the intrinsic chirality and the concentration. The chiral liquid crystal phases have also been investigated using Gay–Berne-type models, in which chirality is encoded in the orientation-dependent potential.[19–21] However, soft and hard spherocylinder models provide a computationally more efficient way to study a variety of liquid crystalline phases.[22–25] Recent studies involving hard helices[26,27–29] have explored the different phases obtained for various molecular chiralities. Dussi *et al.*[30] have used twisted polyhedral-shaped hard particles and obtained entropically

Centre for Condensed Matter Theory, Department of Physics, Indian Institute of Science, Bangalore 560012, India. E-mail: maiti@iisc.ac.in

† Electronic supplementary information (ESI) available. See DOI: https://doi.org/10.1039/d3sm01567j

‡ These authors contributed equally to this work.

§ Current address: Niels Bohr Institute, University of Copenhagen, Blegdamsvej 17, Copenhagen 2100, Denmark.

driven stable chiral nematic phases along with other novel phases. Cholesteric phases are difficult to obtain in numerical simulations as advanced methodologies and large simulation boxes are needed in order to replicate the macroscopic pitch correctly. Hence, many attempts have been made to address this aspect as well. Cinacchi *et al.*[3] have studied the cholesteric phase by considering the hard helix model using both Monte Carlo (MC) and molecular dynamics (MD) simulations and observed the existence of the cholesteric phase in a confined system. Wu and Sun[31,32] have used a flexible chain model where chiral centers are helically arranged on the surface of backbone beads and showed that the pitch of the resultant cholesteric phase depends on the chirality and flexibility of the molecules. Similar results were observed by Tortora and Doye[33] Therefore, the study of the interplay between the microscopic and macroscopic helicity and the underlying interactions is a fascinating field of research.

Interesting traits in spatial ordering and persistent dynamics for the systems of chiral particles appear when activity is incorporated into the system.[34,35] The presence of a wall on the system of chiral active particles is shown to have a rich array of diverse effects.[36] These phenomena appear due to one characteristic of the system: activity. Active matter is driven out of equilibrium by a constant supply of free energy, which is consumed either from the ambient environment or from its own mechanism and dissipates it by performing mechanical work.[37–39] In most cases, activity is *vectorial* in nature due to the force of self-propulsion. However, many physical and biological processes (like chromatin separation in the nucleus[40] and phase separation in colloidal systems) are governed by unequal sharing of available energy and are thus scalar in nature. Such systems can be modeled simply by assigning different diffusivities between the constituents of the system[41] or by coupling them to two different thermostats.[42,43] Such a 'two-temperature model' often results in a phase separation phenomenon termed as 2-TIPS[44] and has been used extensively for the last few years in a diverse setting of systems from Lennard-Jones (LJ) particles,[44,45] polymers,[46,47] dumbbells[48] in our previous works on rod-like particles.[49,50] One of the aims of this study is to explore the effect of the two-temperature model in a system of soft chiral particles.

To validate and benchmark our model of soft helices, we first investigated the equilibrium phase behavior of a system of helical particles with different chiralities. This allowed us to study the dependence of macroscopic pitches on the density and intrinsic pitch of the constituent chiral particles in the presence and absence of a wall in the system. Having established the correct equilibrium phase behavior of the system, we also examined the behavior of a mixture of active and passive helical particles driven by a two-temperature scalar activity. The mixture of particles shows phase separation. The particles in the cold domain experience an ordering transition from isotropic to nematic to the smectic and crystalline structures, whereas the particles in the hot domain remain in the isotropic phase, even when we start from an ordered structure. However, starting from a cholesteric phase, we observe that the activity destabilizes the N_c^* phase by inducing smectic ordering in the cold zone while forming an isotropic structure in the hot zone. At a high enough activity, the smectic ordering in the cold zone eventually transforms into a chiral crystal phase.

The paper is organized as follows: in Section 2, we introduce the model and details of the simulation methods and techniques used. In Section 3, we report various results from equilibrium simulations. We then report the results with the non-equilibrium results – namely the behaviour of a system of active and passive chiral particles, which show the resulting phase separation phenomena (2-TIPS). There is also an ordering transition occurring in the cold zone. Finally, conclusions are drawn along with the main results, and the future outlook of our work is presented in Section 4.

2 Model and simulation methods

Helices can be modeled as a collection of a number of partially overlapping beads of diameter D arranged rigidly around a helical axis $\hat{u}$, which is denoted as the long axis of the molecule (Fig. 1). Our system is made of N such left-handed helical particles with a fixed contour length $L = 10D$. The chirality of a molecule can be defined by the pitch p (the distance after which one bead makes a full rotation around the helical axis) and radius, r, varying, which allows the generation of different helical particles ranging from straight rods to coils (Fig. 2). Our model is similar to that of Kolli *et al.*[25,28] A schematic diagram of the model is presented in Fig. 2.

In our system, two beads belonging to two different particles interact *via* the repulsive part $U(r_{ij})$ of the Lennard-Jones (LJ) potential defined as[51]

$$U(r_{ij}) = \begin{cases} 4\varepsilon\left[\left(\frac{D}{r_{ij}}\right)^{12} - \left(\frac{D}{r_{ij}}\right)^{6}\right] + \varepsilon, & r_{ij} < 2^{1/6}D \\ 0, & r_{ij} \geq 2^{1/6}D, \end{cases} \quad (1)$$

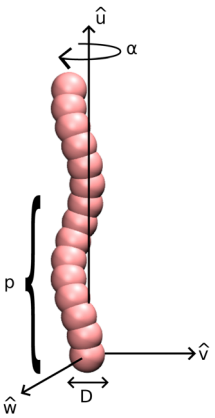

Fig. 1 Schematic details of the left-handed soft helical particles constructed using the beads. The position of the beads rotate around a major axis ($\hat{u}$), in a clockwise fashion as shown by the angle α in the figure, which renders the intrinsic chirality of the molecule to be left-handed. $\hat{v}$ and $\hat{w}$ are the minor or short axis. The pitch p of the particle is the wavelength associated with the helical arrangement of the position of the beads, as shown in the figure. The diameter D of the beads is taken to be 1.0 for our calculations.

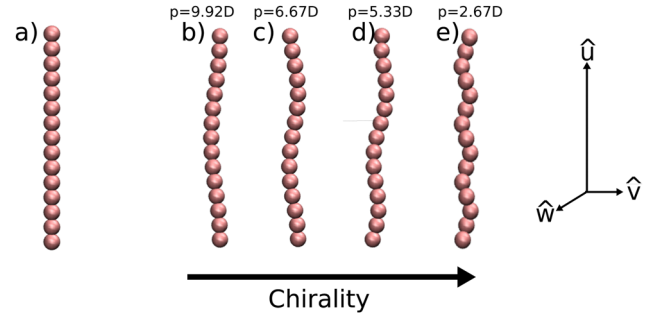

Fig. 2 Schematic diagram of the straight rod made of soft beads in (a). The structures of the left-handed helices of different intrinsic chiralities are shown in (b)–(d), and (e) for the molecular pitches p = 9.92D, 6.67D, 5.33D, and 2.67D respectively, where D is the diameter of one bead. Its long axis is defined by $\hat{u}$ and short axes by $\hat{v}$ and $\hat{w}$, respectively.

where r_{ij} is the distance between the ith and jth atoms belonging to the two different particles, and ε is the unit of energy and denotes the strength of the interaction.

For convenience, the thermodynamic and structural quantities are scaled by the system parameters ε and D and calculated in reduced units, temperature $T^* = k_BT/\varepsilon$, pressure $P^* = P/(k_BT)$, and packing fraction $\eta = \rho v_0$, where $\rho = N/V$ is the number density and v_0 is the effective volume of the helical particle.[25] In Fig. 3, we show that the results obtained from bead model, when used to mimic straight rods, agrees quite well with that of the soft repulsive spherocylinders (SRS).

Obtaining cholesteric phases in computer simulations using the periodic boundary condition (PBC) is a difficult task, as the length scale of the N_c^* phase may be incommensurate with the dimensions of the box. To overcome this issue, we adopt a procedure similar to that of Kolli *et al.*[3] by inserting a wall along a specific direction of the simulation box. The presence of a wall makes the system non-periodic along the wall direction. We inserted a wall on both sides of the $\hat{x}$ direction, which helped the system align and exhibited different liquid crystalline phases. The interaction between the wall and any bead of the helical particles is of the following form:

$$U(r) = \begin{cases} \varepsilon\left[\frac{2}{15}\left(\frac{D}{r}\right)^9 - \left(\frac{D}{r}\right)^3\right] + \varepsilon, & r < 0.4^{1/6}D \\ 0, & r \geq 0.4^{1/6}D, \end{cases} \quad (2)$$

where r is the distance between the wall and any bead.

We built a system of N = 2000 and 10 000 particles in a cubic simulation box using the PACKMOL software.[52,53] Our simulation is done in the following way: first, we equilibrate the system at a certain density. Then, a wall is inserted along one direction (x) taking care to remove particles whose constituent beads overlap with the wall. This lowers the density of the initially built system. We equilibrate such a system for 0.2 million (M) MD steps in an NVT ensemble. Finally, we increase the pressure of the confined system slowly under the NPT ensemble using a semi-isotropic barostat, *i.e.* allowing the simulation box to fluctuate only in the y–z plane. The MD simulations in the NPT ensemble are done using the LAMMPS software.[54] We use rigid body dynamics to integrate the equation of motion with a time step of Δt = 0.001 in reduced units (in units of $D\sqrt{m/\varepsilon}$). The temperature of the system is controlled by the Noose–Hoover thermostat[55,56] with a temperature relaxation time $\tau_T = 100 \times \Delta t$ and pressure is controlled by the semi-isotropic Noose–Hoover barostat with a pressure relaxation time $\tau_P = 1000 \times \Delta t$. We run up to 50 M MD steps to equilibrate the system and another 10 million steps to calculate the thermodynamic quantities.

The cholesteric phase is quantified by calculating the macroscopic pitch P_{chol}. We divide the simulation box along the wall-direction x in a number of slabs and calculate the local nematic director $\hat{n}(x)$ for each of the slabs, which is the eigenvector corresponding to the largest eigenvalue of the traceless symmetric tensor Q defined as

$$Q_{\alpha\beta} = \frac{1}{N}\sum_{i=1}^{N}\frac{3}{2}u_{i\alpha}u_{i\beta} - \frac{1}{2}\delta_{\alpha\beta}. \quad (3)$$

In the above expression, $u_{i\alpha}$ is the αth component of the long axis of the ith particle. The pitch is calculated by fitting the value of $|\hat{n}(0)\cdot\hat{n}(x)|$ to the function $|\cos(qx)|$ where the cholesteric pitch is defined as $P_{chol} = 2\pi/q$. The local nematic director $\hat{n}(x)$ is perpendicular to the helical axis and rotates around it in a helical manner, as shown in the snapshot of Fig. 8(b) where the helical axis is along the x direction.

Next, we incorporate activity into the system using a two-temperature model. We introduce activity by randomly choosing half of the helices and assigning a higher temperature to them while keeping the other particles' temperature fixed at a lower

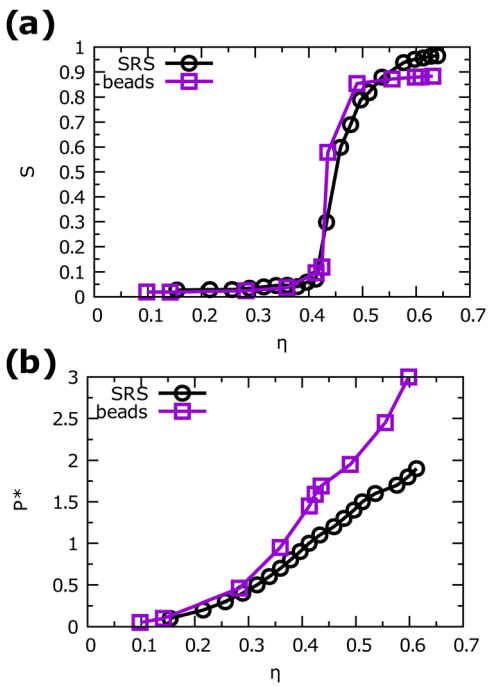

Fig. 3 The phase behavior of rods made of soft beads with an effective aspect ratio A_{eff} = 4.8 is compared to that of soft repulsive spherocylinders. (a) The nematic order parameter S and (b) reduced pressure $P^* = P/k_BT$ are plotted as a function of the packing fraction η for these two models, which match quite well.

value equal to that of the initial equilibrium system. Let T_h^* and T_c^* be the temperatures of the hot and cold particles, respectively. Initially, we equilibrate the system at $T_h^* = T_c^* = 100$, and then increase T_h^* in small steps up to $T_h^* = 20.0$, allowing the system to reach a steady state after each increase in T_h^*, keeping the volume of the simulation box constant throughout the simulation.

We parameterize the activity by

$$\chi = \frac{T_h^* - T_c^*}{T_c^*} \quad (4)$$

For the active case, *i.e.*, for $\chi \neq 0$, we choose the thermostat relaxation time $\tau_T = 0.01$ with an integration time-step $\Delta t = 0.001$ for both types of particles. We run the simulation for 3 M to 4 M integration time steps to reach the steady state and another 1 M steps to calculate thermodynamic and structural quantities.

3 Results and discussion

3.1 Equilibrium properties of soft helical particles

3.1.1 Wall *vs.* no-wall. We simulate the system of soft helical particles under periodic boundary conditions (PBCs) using molecular dynamics (MD) simulations and find that, in the absence of a wall, the system becomes stuck in a jammed state [see (ESI†)[57]], which makes it challenging to obtain liquid crystal ordering within our simulation time. This problem can be overcome by inserting a wall that induces planar alignment, which gives rise to the ordered LC phases. In Fig. 4, we show the effect of the wall on the phase behavior of the system with a molecular pitch $p = 6.67D$. It is observed that the nematic order parameter is very small in the absence of a wall, while it increases with the packing fraction in the presence of a wall. Hence, the equilibrium phase behaviors for different molecular pitches are studied only in the presence of the wall.

3.1.2 Equilibrium phase behavior of different molecular pitches. We compute the equilibrium phase diagram of left-handed helices with different molecular pitches $p = 2.67D$, $5.33D$, $6.67D$ and $9.92D$ with $r = 0.2D$ at a temperature $T^* = 1$. In Fig. 5, we show the different equilibrium phases found for the system with molecular chirality $p = 6.67D$, which are (i) isotropic (I), (ii) cholesteric (N_c^*), (iii) nematic (N), (iv) smectic (Sm) and (v) crystal (K), and present the phase diagram in Fig. 6. The I–N phase transition is determined by calculating the nematic order parameter S, as shown in Fig. 6(b). The cholesteric phase is quantified by calculating the cholesteric pitch P_{chol} as discussed in Section 2. We also calculate the equation of state for the other pitches, as shown in Fig. 7. For $p = 5.33D$, we observe four stable phases for the given range of densities: (i) isotropic, (ii) cholesteric, (iii) nematic, and (iv) smectic. For $p = 9.92D$, we observe three stable phases for the given range of densities: (i) isotropic, (ii) cholesteric, and (iii) smectic. The $I - N_c^*$ transition occurs at a packing fraction $\eta^* \approx 0.30$–0.32. Here, we did not find the existence of a nematic phase. From the cholesteric phase, the system undergoes a phase transition directly to the smectic phase, as can be seen in Fig. 7(c). In the case of molecular pitch $p = 2.67D$, we observe

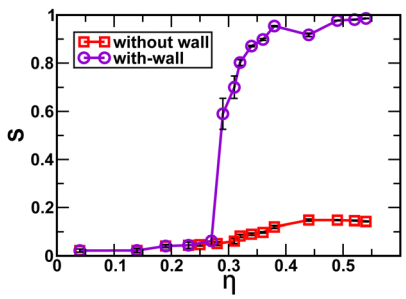

Fig. 4 Nematic order parameter S *vs.* packing fraction η for the pitch $p = 6.67D$ with and without wall. We observe that, in the absence of a wall, the system becomes stuck in a jammed state; hence, the magnitude of the nematic order parameter is very low. The presence of a wall induces planar alignment, which gives rise to ordered liquid crystal phases. Hence, the magnitude of S increases with η.

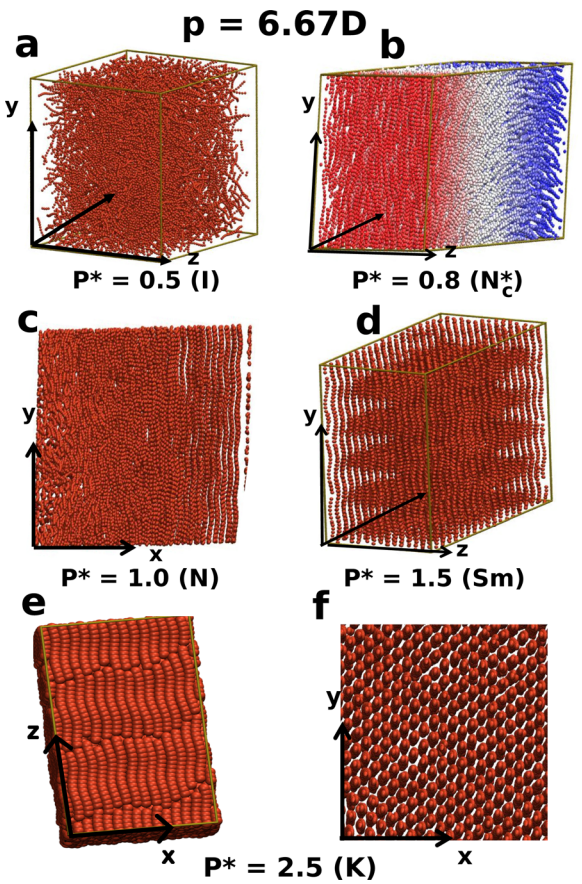

Fig. 5 The equilibrium configurations for the system of soft helical particles with molecular pitch $p = 6.67D$ (the value of D is 1.0), obtained using the wall in the simulations, with increasing pressure. (a) The isotropic, (b) cholesteric, (c) nematic, (d) smectic, and (e), (f) chiral crystal phases are obtained at pressures expressed in the reduced unit $P^* = P\sigma^3/\varepsilon = 0.5$, 0.8, 1.0, 1.5 and 2.5 respectively. In the crystal phase, (e) indicates the positional order along the direction parallel to the layer, and (f) shows the positional ordering within the layers. In the cholesteric structure (b), particles are colored according to their distance from the helical axis ($\hat{x}$) to show the relative rotation of the layers along the helical axis.

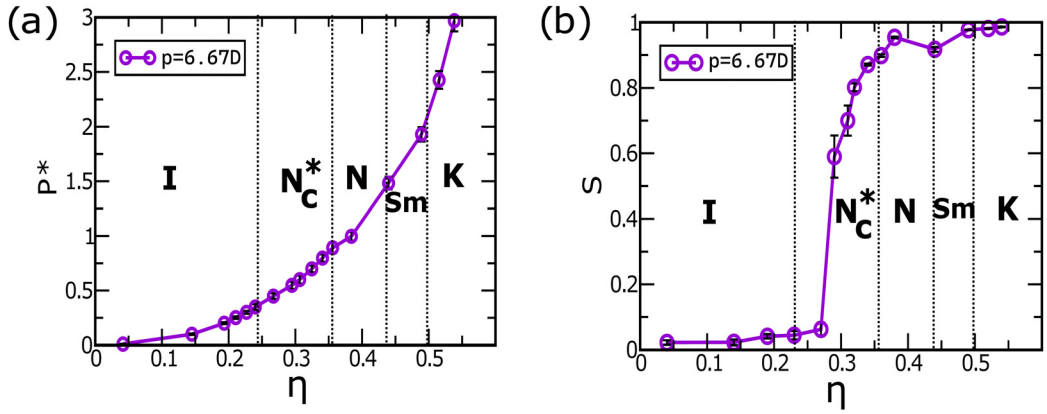

Fig. 6 (a) The equation of state and (b) nematic order parameter S *vs.* packing fraction η for pitch $p = 6.67D$. Here, we obtain five equilibrium phases at a temperature $T^* = 1.0$ for the given range of pressure (P^*): isotropic (I), cholesteric (N_c^*), nematic (N), smectic (Sm) and crystal (K). The dotted lines indicate the coexistence regions near the phase transition points.

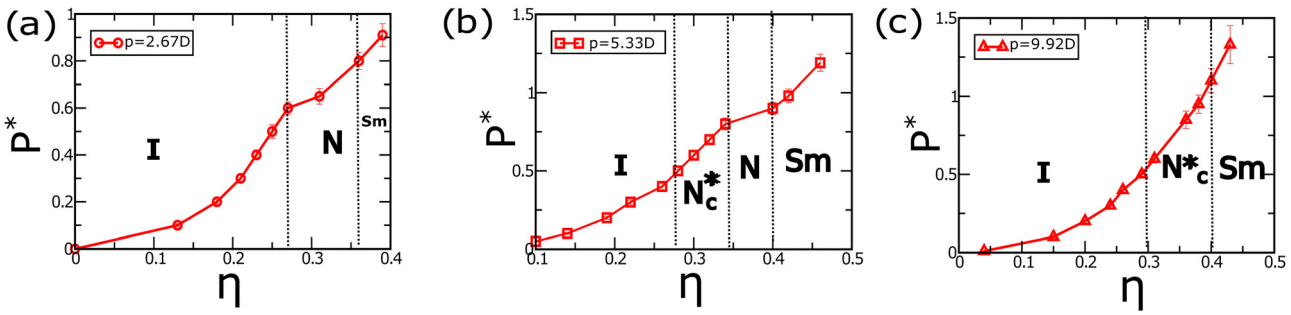

Fig. 7 The equation of state for different molecular pitches: (a) $p = 2.67D$, (b) $p = 5.33D$, and (c) $p = 9.92D$ with $r = 0.20D$ at a temperature $T^* = 1.0$. We find three stable phases for the given range of pressure for $p = 2.67D$: isotropic, nematic, and smectic; four stable phases for pitch $p = 5.33D$: isotropic, cholesteric, nematic and smectic; three stable phases for $p = 9.92D$: isotropic, cholesteric, and smectic. The dotted lines indicate phase boundaries.

three stable phases for the given range of densities: (i) isotropic, (ii) nematic, and (iii) smectic. Here, we did not find an emergence of the cholesteric phase, as shown in Fig. 7(a).

3.1.3 Emergence of a cholesteric phase. We mainly focus on the emergence of a cholesteric phase N_c^* for the aforementioned molecular pitches. In Fig. 8, the configuration of a cholesteric phase is for pitch $p = 9.92D$ for pressure $P^* = 1$, temperature $T^* = 1$ and packing fraction $\eta = 0.4$. In Fig. 9(a), we plot the cosine of the angle θ (the angle between the local nematic director of each slab $\hat{n}(x)$ with that of the slab at $x = 0$, *i.e.* $\hat{n}(0)$) with the distance along the helical axis x and fit it with the function $|\cos(qx)|$. We obtain the magnitude of the cholesteric pitch as $P_{\text{chol}} = 125.66D$ with $q = 0.05$. Our calculated values are in quantitative agreement with the cholesteric pitch reported by Kolli *et al.*[3] ($q = 0.055$) for hard helices using MC simulations. Interestingly, we find the cholesteric phase for pitches, $p = 6.67D$, $5.33D$, which was predicted theoretically earlier by Dijkstra *et al.*[29] In Fig. 9(b), we show the time variation of the pitch for a system with $p = 9.92$ at $P^* = 0.8$. For a given molecular pitch p, P_{chol} decreases with the density, as shown in Fig. 10(a). The magnitude of P_{chol}-also depends on the molecular pitch, p of the helix, as shown in Fig. 10(b). We find that, at a certain packing fraction η, P_{chol} decreases with an

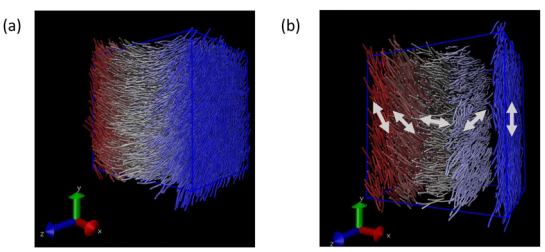

Fig. 8 (a) Configuration of the system in the cholesteric phase for the molecular pitch $p = 9.92D$ at a packing fraction $\eta^* = 0.40$. (b) Configuration of the system divided into a number of slabs. The local nematic director corresponding to each slab is shown by the white arrow. The particles are colored according to their distance along the x-axis: red, blue and gray colors denote the position of the two edges and center of the box respectively along the $\hat{x}$ direction. We see that the local nematic director is rotating around the helical axis ($\hat{x}$). For convenience, only 5 slabs are shown.

increase of the molecular pitch, p. However, more analysis is needed to establish a generalized relationship between microscopic and macroscopic chirality. The cholesteric phase becomes unstable for a very low molecular pitch ($p = 2.67D$), and the system shows a screw-like nematic phase. This

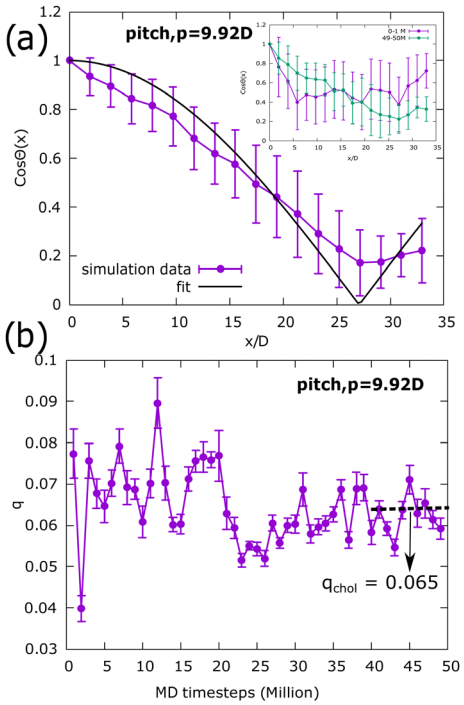

Fig. 9 Determination of the cholesteric pitch P_{chol} for molecular pitch p = 9.92D at packing fraction η = 0.40. (a) The plot of $\cos\theta(x) = |\hat{n}(x)\cdot\hat{n}(0)|$ as a function of the distance along the helical axis $\hat{x}$, where $\hat{n}(x)$ is the local nematic director of each slab located at x. The purple line shows the simulation data and the black smooth curve indicates the linear fitting with the function $|\cos(qx)|$, from which the cholesteric pitch $P_{chol} = 2\pi/q$ is calculated. Inset: Variation of $\cos\theta(x)$ for different time windows (purple curve for initial 0–1M steps, green curve for system at 49–50M steps). (b) The calculated value of q with time for reduced pressure P^* = 0.8. We calculate the cholesteric pitch P_{chol} by taking the average of q for a time window 40–50M, where the fluctuation in the values of q is reduced.

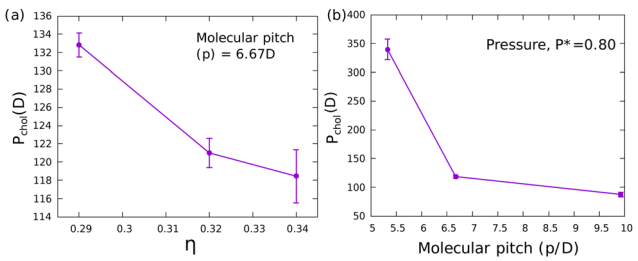

Fig. 10 (a) The dependence of the macroscopic pitch of the cholesteric phase P_{chol} with the packing fraction η for the molecular pitch p = 6.67D. (b) The dependence of the P_{chol} on the molecular pitch p at a specific pressure P^* = 0.8. We see that, for a given molecular pitch p, P_{chol} decreases with an increase of the pressure and for a given pressure, P_{chol} decreases with an increase of the molecular pitch p.

observation is consistent with the results reported by Kolli *et al.*[3,28] for hard helices.

3.2 Activity-induced phase separation

After obtaining the equilibrium phase behavior of the soft helical particles, we investigate how these phase behaviors are affected by scalar activity using the two-temperature model. Starting from a homogeneous isotropic structure, we find the emergence of a 2-TIPS (2-temperature induced phase separation) phenomenon, in which we observe a local phase separation between hot and cold particles that increases with activity till a well-defined interface is formed. In Fig. 11, we show the configuration of the phase-separated structure. The extent of phase separation is quantified by calculating the density order parameter ϕ in the same way as mentioned in our earlier works.[44,45,49,50] Here, we briefly mention it for completeness. We divide the simulation box into a number of sub-boxes N_{box}, and for each sub-box we calculate the number difference between hot n_h and cold n_c particles divided by the total number of particles in each box. We then calculate ϕ by averaging over all the sub-boxes and over a sufficient number of configurations to obtain stable statistics.

$$\phi = \frac{1}{N_{box}}\left\langle \sum_{i=1}^{N_{box}} \frac{|n_c^i - n_h^i|}{(n_c^i + n_h^i)} \right\rangle_{ss}, \quad (5)$$

where $\langle \ldots \rangle_{ss}$ denotes the steady state average of the configurations. ϕ is offset by its initial value in equilibrium at $\chi = 0$.[49] In Fig. 12, we plot ϕ as a function of activities χ for different molecular pitches at the packing fractions η = 0.14, 0.20. These packing fractions correspond to the isotropic phase at equilibrium for the given pitches, as shown in Fig. 6 and 7. We observe that phase separation does not depend much on the molecular pitches. For each packing fraction, the magnitude of ϕ increases with the activities up to a certain value and then saturates, ensuring macroscopic phase separation between hot and cold particles.

3.3 Activity-induced liquid crystal ordering

The hot particles receive a sustained energy flux from the hot bath and transfer it to the cold particles through collisions. Cold particles reject the excess energy to the cold bath, resulting in a steady flow of energy throughout the system.[50] After phase separation, hot particles exert an extra kinetic pressure on the interface, resulting in an ordering transition in the cold zone.[49,50] Starting from a homogeneous isotropic state, we observe cold particles undergoing a phase transition from isotropic to nematic and then other higher-ordered states, while hot particles remain in the isotropic state with a low density. This is interesting as the cold particles show an ordering transition even in the absence of a wall, which is not possible in the equilibrium case as discussed in Section 3.2. Presumably, one can assume that the interface in the active system provides an alignment direction to the cold particles, thus playing the role of the wall in equilibrium.

We quantify the ordering transition by calculating the nematic order parameter of the cold particles S_{cold}, as shown in Fig. 13. We find that S_{cold} increases with increasing activity for the given molecular pitches; however, at a certain activity, S_{cold} have different values for different molecular pitches, indicating different local orderings of the cold particles. For example, at a specific value of χ, p = 5.33D exhibits higher ordering for both densities, while p = 9.92D exhibits lower ordering at η = 0.14 and p = 6.67D exhibits lower ordering at

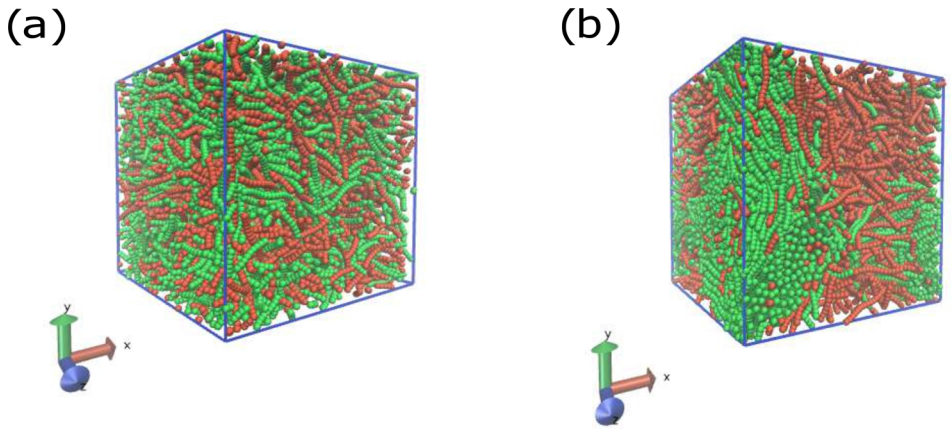

Fig. 11 (a) Equilibrium configuration of N = 2000 soft helical particles with pitch p = 6.67D at the state point (η = 0.20 T^* = 1) in the absence of activity χ = 0. Both hot (red) and cold (green) particles are well mixed at the same temperature. (b) Steady-state configuration after the phase separation at χ = 9. It is clearly visible that the cold particles are segregated and ordered, whereas the surrounding hot particles are disordered.

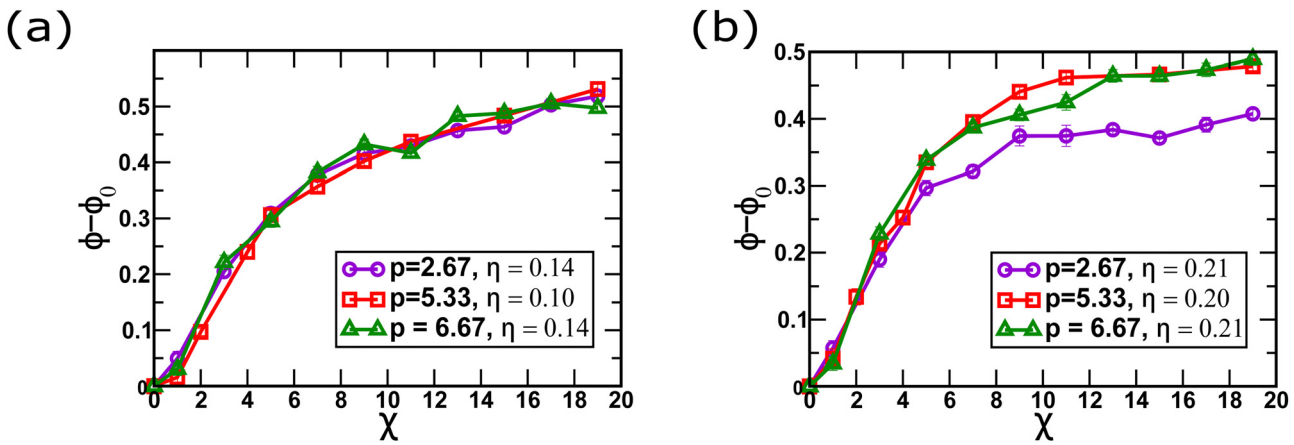

Fig. 12 Density order parameter ϕ *vs.* activity χ for different molecular pitches p (in units of D) at the packing fractions (a) η = 0.14 and (b) η = 0.20. ϕ_0 indicates the magnitude of the density order parameter in the equilibrium system, *i.e.* at χ = 0.

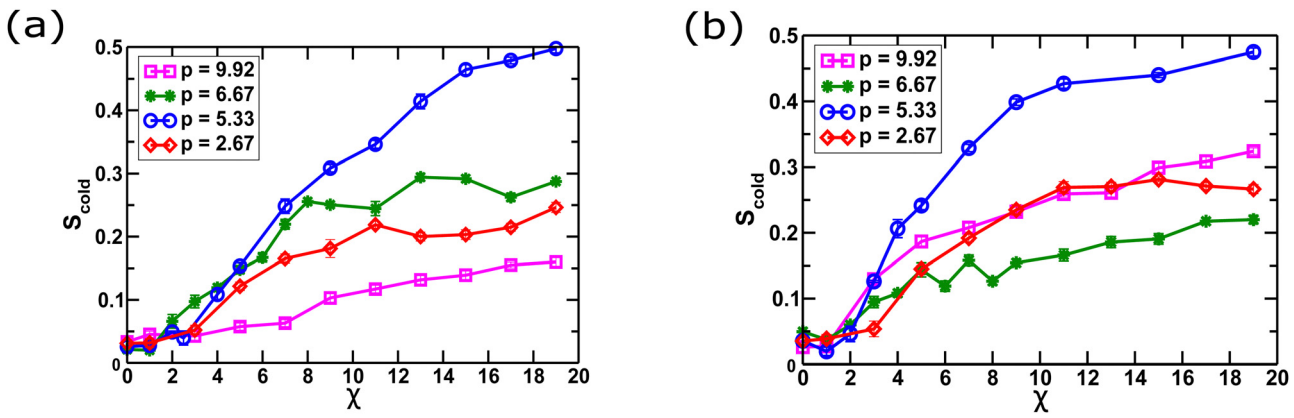

Fig. 13 Nematic order parameter of the cold particles S_{cold} as a function of activity χ for different molecular pitches p at the packing fractions (a) η = 0.14 and (b) η = 0.20. p is expressed in units of D.

η = 0.20. In the case of p = 9.92D, we perform a two-temperature simulation in the presence of the wall, where we find better ordering. In Fig. 14, we observe that for p = 9.92D, S_{cold} increases drastically in the presence of the wall than that of the system without a wall at the same activity. Thus, the wall also promotes higher ordering in the active cases.

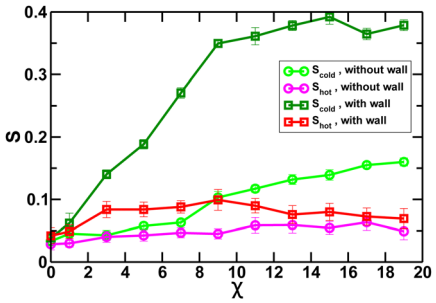

Fig. 14 Nematic order parameters of the cold S_{cold} and hot S_{hot} particles with and without a wall with activity χ for the pitch $p = 9.92D$ at a packing fraction $\eta = 0.14$. We observe that S_{cold} increases in the presence of the wall.

3.4 Breakdown of the cholesteric phase

Starting from a cholesteric phase, we observe that the activity destabilizes the cholesteric phase by driving the cold particles through a phase transition to the next higher-ordered state and the hot particles to a state of less order. This result is consistent with our previous work on SRS, as mentioned in ref. 49,50. In Fig. 15(b), we see that, for $p = 6.67D$, the cold particles form a smectic phase while the hot zone shows an isotropic structure. The breakdown of the N_c^* phase is quantified by plotting $\cos\theta(x)$ with the distance perpendicular to the hot–cold interface (θ is the relative angle between the local nematic directors at a slab x and at $x = 0$, see Section 3.1.3). Fig. 15(c) shows the behaviour of $\cos\theta(x)$ for the initial cholesteric structure, whereas in Fig. 15(d), we see that $\cos\theta(x)$ is homogeneous in the segregated cold-dominated zone, indicating the disappearance of the cholesteric phase. At a high enough activity, the smectic ordering in the cold zone eventually transforms into a chiral crystal phase.

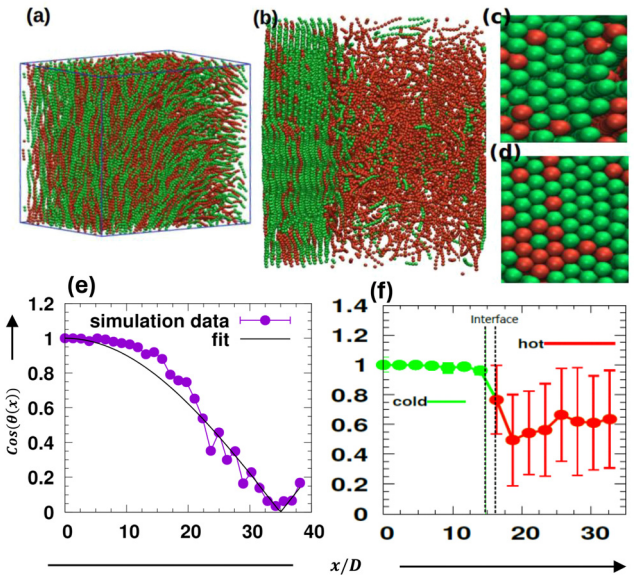

Fig. 15 Breakdown of the cholesteric phase for molecular pitch $p = 6.67D$ at pressure $P^* = 0.55$. (a) Initial configuration at $\chi = 0$, indicating the cholesteric phase. (b) Configuration of the phase-separated system at $\chi = 14$. (c) Positions of the top beads of the molecules within a layer in the smectic-like phase, and (d) the positional ordering of the top beads of the molecules within a layer in the higher-ordered chiral crystal phase. The cold and hot particles are represented by green and red colors, respectively. Calculation of the cholesteric pitch P_{chol} for (e) $\chi = 0$ and (f) $\chi = 14$. In equilibrium, $P_{chol} = 133D$, and $\cos\theta(x)$ is homogeneous in the segregated zone, as shown in (d).

Similar phenomena have been observed when we start from an initial cholesteric phase for a system of particles with microscopic pitch $p = 9.92D$. Starting with a cholesteric phase at pressure $P^* = 0.9$, we introduce activity into the system using the two-temperature model. We observe a phase separation between active and passive particles. There is a fraction of cold particles trapped inside the hot zone and a fraction of hot particles trapped inside the cold zone. The ordering of cold or passive particles gradually increases with activity, but cholesteric ordering cannot persist in the region, whereas the hot particles form a disordered isotropic phase (see (ESI†)[57]). A smectic layering occurs in the cold domain. The isotropic phase forms at the interior of the system, whereas the smectic domain forms close to the walls. Therefore, we conclude that the disappearance of the cholesteric phase with the introduction of scalar activity is a universal phenomenon as far as different microscopic pitches are concerned.

4 Conclusion and future outlook

In this work, we examined the effect of chirality on the phase behavior of equilibrium and active helical particles driven by two-temperature scalar activity. We first construct an equation of state for soft helical rod-like particles of various intrinsic chiralities using molecular dynamics (MD) simulations. We observe the occurrence of ordered nematic (N) and cholesteric (N_c^*) phases in the presence of a wall for various values of molecular pitch p, namely $p = 9.92D$, $6.67D$ and $5.33D$. Next, we introduce an activity into the system using a two-temperature model. Starting from a homogeneous isotropic (I) phase, we find that the activity causes the hot and cold particles to phase-separate and the cold particles to undergo an ordering transition even in the absence of a wall. This observation unveiled that the hot–cold interface in the active system acts as a wall in equilibrium by giving the cold particles some alignment directions. However, starting from a cholesteric phase, the activity destabilizes the N_c^* phase by inducing smectic ordering in the cold zone and the isotropic structure in the hot zone. Smectic (Sm) ordering in the cold zone eventually transforms into a chiral crystal phase at a high enough activity.

The future outlook of this work is as follows: in equilibrium, another interesting prospect would be to determine the handedness of the macroscopic cholesteric phase and how they depend on the density and chirality of the constituent particles. It would be interesting to explore a full phase diagram using molecular dynamics simulations. The existence of a cholesteric phase for systems with microscopic pitches, which has not been reported earlier, also calls for an extensive study on the equilibrium properties of such systems. A similar model can

also be used to study emerging phases in a collection of chiral active swimmers.[58]

Author contributions

Jayeeta Chattopadhyay and Jaydeep Mandal: conceptualization, methodology, investigation, visualization, formal analysis, and writing. Prabal K. Maiti: conceptualization, visualization, supervision, writing – review and editing. The manuscript was written through equal contribution from all authors.

Conflicts of interest

There are no conflicts to declare.

Acknowledgements

JC thanks DST, India, and JM thanks MHRD, India, for the fellowship. PKM thanks DST, India, for financial support and SERB, India, for funding and computational support.

Notes and references

1 P.-G. De Gennes and J. Prost, *The physics of liquid crystals*, Oxford university press, 1993, vol. 83.
2 S. Dussi and M. Dijkstra, *Nat. Commun.*, 2016, **7**, 1–10.
3 G. Cinacchi, A. Ferrarini, A. Giacometti and H. B. Kolli, *J. Chem. Phys.*, 2017, **147**, 224903.
4 M. Nakata, G. Zanchetta, B. D. Chapman, C. D. Jones, J. O. Cross, R. Pindak, T. Bellini and N. A. Clark, *Science*, 2007, **318**, 1276–1279.
5 G. Zanchetta, F. Giavazzi, M. Nakata, M. Buscaglia, R. Cerbino, N. A. Clark and T. Bellini, *Proc. Natl. Acad. Sci. U. S. A.*, 2010, **107**, 17497–17502.
6 T. P. Fraccia, G. P. Smith, L. Bethge, G. Zanchetta, G. Nava, S. Klussmann, N. A. Clark and T. Bellini, *ACS Nano*, 2016, **10**, 8508–8516.
7 Z. Dogic and S. Fraden, *Curr. Opin. Colloid Interface Sci.*, 2006, **11**, 47–55.
8 G. Nyström, M. Arcari and R. Mezzenga, *Nat. Nanotechnol.*, 2018, **13**, 330–336.
9 R. S. Werbowyj and D. G. Gray, *Mol. Cryst. Liq. Cryst.*, 1976, **34**, 97–103.
10 R.-D. Gilbert and P. Patton, *Prog. Polym. Sci.*, 1983, **9**, 115–131.
11 F. Tombolato, A. Ferrarini and E. Grelet, *Phys. Rev. Lett.*, 2006, **96**, 258302.
12 P. J. Collings, *Liquid crystals: nature's delicate phase of matter*, Princeton University Press, 2002.
13 F. Livolant and M. F. Maestre, *Biochemistry*, 1988, **27**, 3056–3068.
14 S. Saurabh, Y. Lansac, Y. H. Jang, M. A. Glaser, N. A. Clark and P. K. Maiti, *Phys. Rev. E*, 2017, **95**, 032702.
15 S. Naskar, S. Saurabh, Y. H. Jang, Y. Lansac and P. K. Maiti, *Soft Matter*, 2020, **16**, 634–641.
16 J. P. Straley, *Phys. Rev. A: At., Mol., Opt. Phys.*, 1976, **14**, 1835.
17 T. Odijk, *J. Phys. Chem.*, 1987, **91**, 6060–6062.
18 R. A. Pelcovits, *Liq. Cryst.*, 1996, **21**, 361–364.
19 R. Memmer, H.-G. Kuball and A. Schönhofer, *Liq. Cryst.*, 1993, **15**, 345–360.
20 S. Sarman and A. Laaksonen, *Phys. Chem. Chem. Phys.*, 2013, **15**, 3442–3453.
21 T. Paul and J. Saha, *Phys. Rev. Res.*, 2019, **1**, 032012.
22 P. Bolhuis and D. Frenkel, *J. Chem. Phys.*, 1997, **106**, 666–687.
23 Y. Lansac, P. K. Maiti, N. A. Clark and M. A. Glaser, *Phys. Rev. E: Stat., Nonlinear, Soft Matter Phys.*, 2003, **67**, 011703.
24 P. K. Maiti, Y. Lansac, M. A. Glaser and N. A. Clark, *Phys. Rev. Lett.*, 2002, **88**, 065504.
25 E. Frezza, A. Ferrarini, H. B. Kolli, A. Giacometti and G. Cinacchi, *J. Chem. Phys.*, 2013, **138**, 164906.
26 S. N. Fejer, D. Chakrabarti and D. J. Wales, *Soft Matter*, 2011, **7**, 3553–3564.
27 H. B. Kolli, E. Frezza, G. Cinacchi, A. Ferrarini, A. Giacometti and T. S. Hudson, *J. Chem. Phys.*, 2014, **140**, 081101.
28 H. B. Kolli, E. Frezza, G. Cinacchi, A. Ferrarini, A. Giacometti, T. S. Hudson, C. De Michele and F. Sciortino, *Soft Matter*, 2014, **10**, 8171–8187.
29 S. Belli, S. Dussi, M. Dijkstra and R. van Roij, *Phys. Rev. E: Stat., Nonlinear, Soft Matter Phys.*, 2014, **90**, 020503.
30 S. Dussi and M. Dijkstra, *Nat. Commun.*, 2016, **7**, 1–10.
31 L. Wu and H. Sun, *Soft Matter*, 2018, **14**, 344–353.
32 L. Wu and H. Sun, *Phys. Rev. E*, 2019, **100**, 022703.
33 M. M. Tortora and J. P. Doye, *Mol. Phys.*, 2018, **116**, 2773–2791.
34 F. J. Sevilla, *Phys. Rev. E*, 2016, **94**, 062120.
35 Z.-F. Huang, A. M. Menzel and H. Löwen, *Phys. Rev. Lett.*, 2020, **125**, 218002.
36 L. Caprini and U. M. B. Marconi, *Soft Matter*, 2019, **15**, 2627–2637.
37 M. C. Marchetti, J. F. Joanny, S. Ramaswamy, T. B. Liverpool, J. Prost, M. Rao and R. A. Simha, *Rev. Mod. Phys.*, 2013, **85**, 1143–1189.
38 S. Ramaswamy, *Annu. Rev. Condens. Matter Phys.*, 2010, **1**, 323–345.
39 G. S. Redner, M. F. Hagan and A. Baskaran, *Phys. Rev. Lett.*, 2013, **110**, 055701.
40 N. Ganai, S. Sengupta and G. I. Menon, *Nucleic Acids Res.*, 2014, **42**, 4145–4159.
41 S. N. Weber, C. A. Weber and E. Frey, *Phys. Rev. Lett.*, 2016, **116**, 058301.
42 A. Y. Grosberg and J.-F. Joanny, *Phys. Rev. E: Stat., Nonlinear, Soft Matter Phys.*, 2015, **92**, 032118.
43 A. Y. Grosberg and J.-F. Joanny, *Polym. Sci., Ser. C*, 2018, **60**, 118–121.
44 N. Venkatareddy, J. Mandal and P. K. Maiti, *Soft Matter*, 2023, **19**, 8561–8576.
45 S. S. N. Chari, C. Dasgupta and P. K. Maiti, *Soft Matter*, 2019, **15**, 7275–7285.
46 J. Smrek and K. Kremer, *Phys. Rev. Lett.*, 2017, **118**, 098002.
47 J. Smrek and K. Kremer, *Entropy*, 2018, **20**, 520.
48 N. Venkatareddy, S.-T. Lin and P. K. Maiti, *Phys. Rev. E*, 2023, **107**, 034607.

49 J. Chattopadhyay, S. Pannir-Sivajothi, K. Varma, S. Ramaswamy, C. Dasgupta and P. K. Maiti, *Phys. Rev. E*, 2021, **104**, 054610.
50 J. Chattopadhyay, S. Ramaswamy, C. Dasgupta and P. K. Maiti, *Phys. Rev. E*, 2023, **107**, 024701.
51 J. D. Weeks, D. Chandler and H. C. Andersen, *J. Chem. Phys.*, 1971, **54**, 5237–5247.
52 L. Martnez, R. Andrade, E. G. Birgin and J. M. Martnez, *J. Comput. Chem.*, 2009, **30**, 2157–2164.
53 J. M. Martnez and L. Martnez, *J. Comput. Chem.*, 2003, **24**, 819–825.
54 S. Plimpton, *J. Comput. Phys.*, 1995, **117**, 1–19.
55 S. Nosé, *Mol. Phys.*, 1984, **52**, 255–268.
56 W. G. Hoover, *Phys. Rev. A: At., Mol., Opt. Phys.*, 1985, **31**, 1695–1697.
57 ESI†.
58 V. Semwal, J. Joshi, S. Dikshit and S. Mishra, *Phys. A*, 2024, **634**, 129435.